

Iron and Hydrogen – Characterization of Fe-H Bonding in Hydrogenases and Model Compounds Using Nuclear Resonant Vibrational Spectroscopy (NRVS)

1. Introduction

Molecular hydrogen, H₂, has been offered as an ideal carbon-free energy carrier, and a sustainable ‘hydrogen economy’ without CO₂ emissions is one approach to mitigating climate change. Nowadays, most industrial H₂ is produced by high-temperature steam reforming of natural gas which leads to the release of at least one molecule of CO₂ for every four molecules of H₂ produced. An ideal ‘hydrogen economy’ would use electrochemical energy from solar or other carbon-free sources to drive the water-splitting ‘hydrogen evolution reaction’ (HER). The ‘green hydrogen’ would be consumed in fuel cells to produce electricity for a ‘decarbonized’ economy.

At the moment, the best human-made catalysts for producing or consuming H₂ rely on precious and rare platinum (Pt). In fact, the 2020 SPring-8 Research Frontiers contained an excellent review by Iwasawa of synchrotron-based Pt fuel cell research. Over the long term, better H₂-processing catalysts from earth-abundant materials could play an essential part of H₂ ‘decarbonization’ plans. One source of inspiration is Nature, which employs hydrogenase (H₂ase) enzymes that are as fast as the best Pt catalysts, but use plentiful Fe or Ni at their active sites. H₂ uptake and production in these enzymes is catalyzed by two types of H₂ases, [FeFe] H₂ase [1] and [NiFe] H₂ase [2].

The active site for [FeFe] H₂ases is an ‘H-cluster’, which has an iron-

sulfur [4Fe–4S]_H subcluster linked by a cysteine thiolate to an organometallic [2Fe]_H subcluster (Fig. 1(a)) [1]. The active site in [NiFe] H₂ases (Fig. 1(b)) [2] has a Ni linked to Fe by a pair of cysteine thiolate (S) ligands with two more terminal cysteine thiolate (S) ligands.

The H₂ase active sites are buried in protein matrices which have specific amino acid channels for transporting protons and additional Fe–S clusters for moving electrons (Fig. 2). This is elegant protein engineering, but it also means that the active sites in enzyme solutions are quite dilute, on the order of 1 mM or less. This constrains the types of methods that can be used to study these enzymes.

Detailed knowledge about the structures and catalytic mechanisms of H₂ases is important for using the enzymes themselves or for building synthetic catalysts that mimic their properties. Although crystal structures are available for many of these enzymes, the intermediates with bound H have not been crystallized. We thus resort to spectroscopic methods. One key goal for understanding these

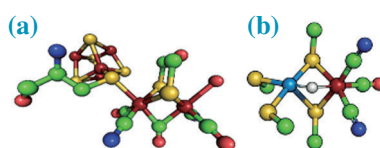


Fig. 1. (a) The [FeFe] H₂ase H-cluster. (b) The [NiFe] H₂ase active center. Color scheme: Fe, Ni, S, C, N, O, H.

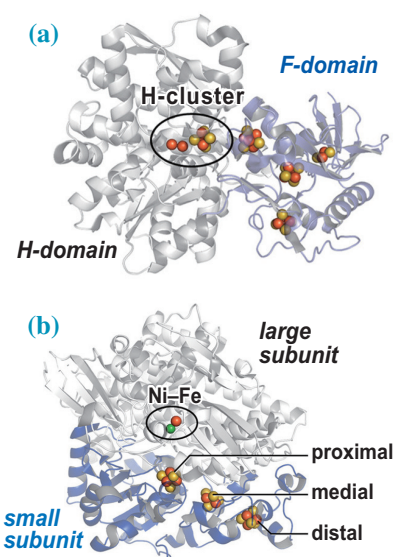


Fig. 2. (a) The [FeFe] H₂ase protein. (b) The [NiFe] H₂ase protein. Color scheme: Fe, Ni, S.

enzymes is to document how H is bound to Fe in various intermediate states.

Vibrational spectroscopy is commonly used by chemists to unravel the structures of unknown species, and the two most familiar approaches are infrared (IR) and resonance Raman (RR) techniques. In fact, IR has been used to study the CO and CN stretching modes in H₂ases, and RR has been used to record Fe–S stretches. However, Fe–H vibrations are too weak to see by IR, and H-bound complexes are too photosensitive for RR. We have thus turned to a synchrotron-based method, Nuclear Resonant Vibrational Spectroscopy (NRVS).

2. Nuclear Resonance Vibrational Spectroscopy

In an NRVS experiment one observes vibrational transitions that occur as sidebands of a nuclear transition (Fig. 3). An ultra-high energy resolution monochromator is required, because vibrational linewidths are on the order of 0.5 meV (4 cm^{-1}) compared to the photon energy (for ^{57}Fe) of 14.4 keV! A very fast gated APD detector is required to see the very small fraction of nuclear events in a background of electronic events that is many orders of magnitude higher (Fig. 3). These requirements were initially met at SPring-8 BL09XU, where we began and first developed our NRVS experiments with the help of staff scientist Yoshitaka Yoda. Later, with the help of Dr. Yoda, we moved some experiments to beamline BL19LXU, to take advantage of the higher flux on a multi-undulator beamline.

For bioinorganic chemistry experiments, NRVS has several advantages over traditional vibrational spectroscopies. In the case of ^{57}Fe NRVS, one observes only vibrations which involve motion of the ^{57}Fe nucleus. Thus, although proteins have thousands of normal modes, ^{57}Fe NRVS allows us to focus on the important modes which involve ^{57}Fe motion. Furthermore, biochemists have developed techniques for labeling, for example, just the $[\text{2Fe}]_{\text{H}}$ subsite of $[\text{FeFe}]_{\text{H}_2\text{ase}}$. This allows us to plan

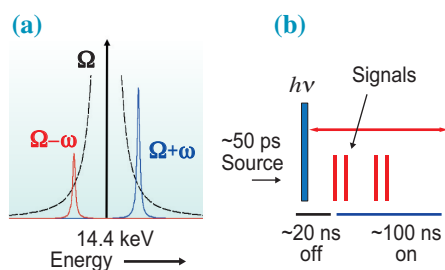


Fig. 3. (a) Energies involved in NRVS. The ^{57}Fe Mössbauer transition is at Ω . The vibrational energies ω are on the order of 10–100 meV. (b) The timing scheme that allows detection of NRVS. The ^{57}Fe excited state lifetime is $\sim 100\text{ ns}$. Detectors are turned off to reject the ‘prompt’ pulses and then turned back on to capture delayed nuclear events.

exquisitely selective experiments that focus on modes involving the enzyme active site. With sufficient signal averaging, we can even see vibrations with relatively little ^{57}Fe motion, such as Fe–H bending and stretching modes.

3. [NiFe] Hydrogenase Studies: Fe–H–Ni Wagging Modes

Our earliest hydrogenase work involved the $[\text{NiFe}]_{\text{H}_2\text{ase}}$ from *Desulfovibrio vulgaris* Miyazaki F (*DvMF*). We first reported the ability to see typical Fe–CO and Fe–CN bending and stretching modes [3]. More exciting, with extensive signal averaging, we were able to discern a Fe–H–Ni wagging mode that confirmed the presence of a hydride bridge in the most reduced Ni–R form of this enzyme (Fig. 4) [2]. Key to the success of this measurement was the extra flux available on the extra-long undulator beamline BL19LXU.

The existence and location of this band provided a critical reference point for selecting the likely structure of the $[\text{NiFe}]$ center in the ‘form R’ state from at least 12 models considered by density function theory (DFT) calculations [2]. Of course, all the Fe–CN and Fe–CO features were also constraints for the DFT simulations. We are now conducting similar studies on the regulatory and the membrane-bound $[\text{NiFe}]_{\text{H}_2\text{ases}}$ from *Ralstonia eutropha* (*ReRH* and *ReMBH*) [4,5].

4. [FeFe] Hydrogenase Studies: Fe–H Bending Modes

With $[\text{FeFe}]_{\text{H}_2\text{ases}}$, H_2 bond activation occurs at the Fe_d site in the $[\text{2Fe}]_{\text{H}}$ sub-cluster distal to the $[\text{4Fe4S}]_{\text{H}}$ cluster. At this site the aminodithiolate (ADT) group plays a fundamental role in H^+ transfer to a proton relay to the protein exterior (Fig. 5). Thanks to developments in artificial maturation, our collaborators were able to replace the NH of the ADT bridge in the *Cr-HydA1* $[\text{2Fe}]_{\text{H}}$ subcluster with an O to form an oxodithiolate (ODT) variant. This replacement obstructs the H^+ transport chain, which is one approach to trapping

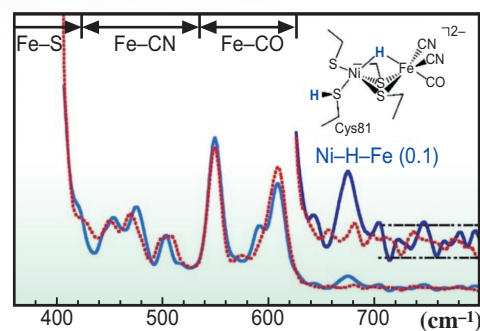


Fig. 4. NRVS PVDOS for *DvMF* $[\text{NiFe}]_{\text{H}_2\text{ase}}$ in H_2O (—) versus D_2O (---) showing a Ni–H–Fe wagging mode at 675 cm^{-1} (signal $\sim 0.1\text{ cts/s}$). The top right insert is the best DFT model obtained *via* simulating the observed NRVS.

a transient intermediate known as H_{hyd} .

Another type of variant involves mutagenesis of Cys to Ser at position 169, thus changing the functional group adjacent to the H-cluster from $-\text{SH}$ to $-\text{OH}$ (Fig. 5). The C169S enzyme has a 100-fold reduction in catalytic activity compared to native *Cr-HydA1*, presumably due to less efficient transfer of H^+ to the H-cluster [1]. We have examined the H_{hyd} forms of the ODT variant, the C169S variant, and wild-type enzyme by NRVS, and the spectra for these three species are compared in Fig. 6.

As seen in Fig. 6, the NRVS signature for the terminal X–Fe–H bending motion in the H_{hyd} state exhibits two main bands in the $650\text{--}750\text{ cm}^{-1}$ range. From DFT calculations these are rationalized as arising from H^- motion perpendicular and parallel to the N- $[\text{2Fe}]_{\text{H}}$ plane (Fig. 7). Since the

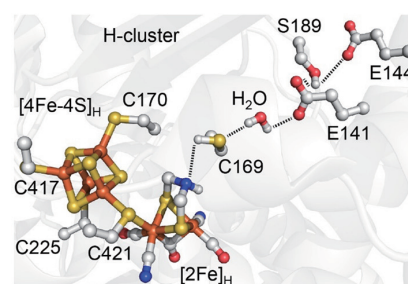


Fig. 5. The proton transfer chain in $[\text{FeFe}]_{\text{H}_2\text{ase}}$ from *Chlamydomonas reinhardtii* – *CrHydA1*.

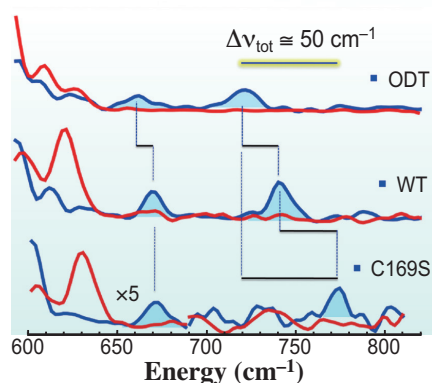


Fig. 6. NRVS PVDOS in the X–Fe–H region for H₂ase samples in the H_{hyd} form, in H₂O (—) vs D₂O (—): ODT variant (top), wild-type (middle), and C169S (bottom).

nitrogen of the ADT bridge is involved in transporting solvent protons H⁺ to and from Fe_d through the relay of conserved amino acids that lead to the surface of the protein, understanding the motion of the Fe–H with respect to that N is directly relevant to the catalytic mechanism.

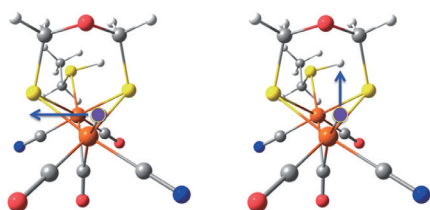


Fig. 7. Direction of hydride motion (labeled \rightarrow) associated with lower frequency (left) and higher frequency (right) bending modes seen in NRVS.

We found a significant shift to higher frequency in the X–Fe–H in-plane bending mode of C169S *Cr*-HydA1 (772 cm⁻¹) compared to the native protein (744 cm⁻¹) and ODT variant *Cr*-HydA1 (727 cm⁻¹) (Fig. 6) [1,6,7]. The large upshift of C169S band in comparison with the native enzyme is rationalized by DFT calculations to be caused by stronger interaction between the –OH of C169S with the bridgehead –NH– of the active site in comparison with the –SH/–NH– in the native enzyme. In contrast, the lower energy band, produced by the localized ‘out-of-plane’ normal mode,

is essentially a pure Fe_d–H bending motion which is decoupled from other nuclei. Thus, the out-of-plane wagging modes have about the same frequency (670–675 cm⁻¹) for all three variants.

5. [FeFe] H₂ase with Labeled ADT: Low Frequency Modes

Site-selective labeling of the [2Fe]_H subcluster alone enables other interesting features to be observed. For example, a pair of synthetic diiron precursor isotopologues were used to reconstitute the H-cluster of *Cr*-HydA1 [FeFe] H₂ase: one of them was labeled with –¹³CD₂–ADT while the other had natural abundance –CH₂–ADT (Fig. 8) [6]. NRVS was measured on samples poised in the catalytically crucial H_{hyd} state containing a terminal hydride at the distal Fe_d site. The spectral effect of –¹³CD– vs –CH₂– were observed in NRVS for this pair of H_{hyd} enzymes.

Among the differences in various locations, small shifts in the X–Fe–H wagging and in-plane bending modes were observed. Of special interest, changes in modes as low as 160 cm⁻¹ were also observed (Fig. 9). DFT simulations of the spectra allowed identification of the ⁵⁷Fe motion coupled to the ADT ligand motions. A variety of normal modes involve shortening of the distance between the distal Fe–H hydride and ADT NH bridgehead hydrogen. These are presumed to be ‘rate-promoting vibrations’ which may be relevant to the formation of a transition state on the way to H₂ formation.

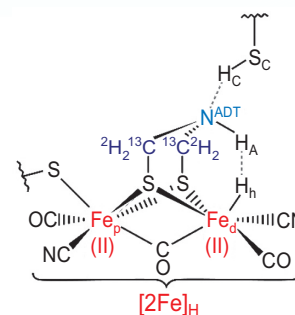


Fig. 8. Labeling of ADT ligand that allowed confirmation of assignments.

6. H–Fe–H₂ Model Complexes: Fe–H and Fe–H₂ Stretching

In addition to Fe–H bending or wagging features, Fe–D or Fe–H stretching features at higher energies can provide additional information to constrain DFT calculations of proposed structural models. As preparation for observing Fe–H/D stretching in enzyme samples, we have examined these features in various model complexes [2,8]. At the highest energy for NRVS to date, we looked for Fe–H stretching modes in *trans*-[⁵⁷Fe(η²-H₂)(H)(dppe)₂] [BPh₄] (Fig. 11) [8]. The vibrational modes associated with the NRVS peaks at 1774 and 1915 cm⁻¹ were assigned: the former is the asymmetric Fe–H stretching mode from the Fe(H₂) component, while the latter is the Fe–H stretching from the FeH bond. These features will be useful standards for Fe(H₂) or FeH structures in planned searches for Fe(H₂) bonding in H₂ase samples. The peak at 1956 cm⁻¹ is the

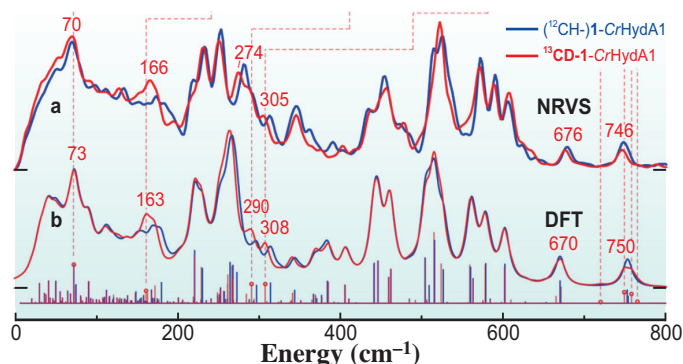


Fig. 9. Observed and calculated NRVS PVDOS.

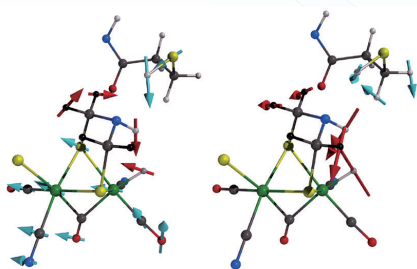


Fig. 10. Left: a low frequency mode calculated at 73 cm^{-1} . Right: a high frequency mode calculated at 758 cm^{-1} . Both modes bring Fe–H and N–H closer together (and also involve C169 S–H). Color scheme: Fe, S, C, N, O, H.

Fe–H stretching mode from a byproduct when H_2 dissociates. This is the highest energy NRVS band observed to date.

7. A summary of what we have learned so far

The NRVS results so far, combined with DFT simulations to interpret the data, have revealed important information about H_2 ases that was not available from X-ray diffraction or other spectroscopies. First, we have seen that [FeFe] H_2 ases bind hydrides exclusively as terminal ligands, as opposed to the bridging form used by [NiFe] H_2 ases. Second, we have seen that the dynamics of the terminal hydride are exquisitely sensitive to both the nature of the dithiolate bridging ligand and to the sidechain of the amino acid in the 169 position (*CrHydA1* numbering, Fig. 5). Third, we have seen

evidence for potential ‘rate-promoting vibrations’ in which flexing of the ADT bridgehead N combined with Fe–H bending brings the two H atoms closer for formation of H_2 bonding. Finally, we have seen that the –SH group of the Cys169 thiolate is actively involved in many of the normal modes which also exhibit ADT and Fe–H motions. This tells synthetic chemists seeking to mimic H_2 ase properties that structures as far as 5 Å from the Fe_d active site are relevant for the initial steps in catalytic activity.

8. Where is this research going?

Where is this research going? Our current goal is to capture the earliest steps in the H_2 splitting reaction, which many believe is a fleeting Fe– H_2 complex for the [FeFe] enzyme. Since this intermediate presumably quickly splits into a hydride and a proton, our plan is to capture it at low temperature. H_2 will be generated photochemically from NH_3BH_3 and a nanoparticle catalyst, and the H_2 ase will be stabilized in a cryosolvent at low temperatures. We plan to monitor the photochemistry with *in situ* IR spectroscopy.

This research has benefited from the continuing improvement in the emittance of the SPring-8 storage ring, the brightness available from improved undulators, the stability of high-resolution monochromators, and better avalanche photodiode detectors. A mobile NRVS apparatus that Dr. Yoshitaka Yoda and his colleagues

made to use at other beamlines (e.g., BL19LXU) has also been critical for making this research possible.

9. Other groups now using NRVS at SPring-8

NRVS has become popular with other groups around the world, some of whom have initially collaborated with us and now run vigorous independent programs. The group of Prof. Solomon at Stanford has at least 10 NRVS publications – we cite just one recent example [9]. The groups of Prof. Oliver Lenz at Technical University of Berlin, Dr. Serena DeBeer at the Max Planck Institute in Mulheim and Dr. Artur Braun at the Empa - Swiss Federal Laboratories are also active users of SPring-8 NRVS capabilities. The demand for NRVS capabilities, not only for ^{57}Fe but also for other isotopes, is rapidly growing and speaks to a productive future for this technique.

Hongxin Wang^a and Stephen P. Cramer^{a,b,*}

^aSETI Institute, Mountain View, USA

^bUniversity of California, Davis, USA

*Email: scramer@seti.org

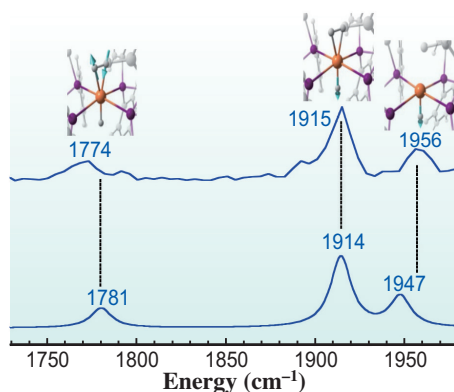


Fig. 11. NRVS PVDOS and DFT calculations for $\text{trans-}[^{57}\text{Fe}(\eta^2\text{-H}_2)(\text{H})(\text{dppe})_2][\text{BPh}_4]$.

References

- [1] C.C. Pham *et al.*: *Angew. Chem. Int. Ed.* **57** (2018) 10605.
- [2] H. Ogata *et al.*: *Nat. Comm.* **6** (2015) 7890.
- [3] S. Kamali *et al.*: *Angew. Chem. Int. Ed.* **52** (2013) 724.
- [4] G. Caserta *et al.*: *Chem. Sci.* **12** (2021) 2189.
- [5] C. Lorent *et al.*: *Angew. Chem. Int. Ed.* **60** (2021) 15854.
- [6] V. Pelmeshnikov *et al.*: *J. Am. Chem. Soc.* **143** (2021) 8237.
- [7] V. Pelmeshnikov *et al.*: *J. Am. Chem. Soc.* **139** (2017) 16894.
- [8] M.H. Chiang *et al.*: *Inorg. Chem.* **60** (2021) 555.
- [9] A.B. Jacobs *et al.*: *J. Am. Chem. Soc.* **143** (2021) 16007.